EuroSun 2026

TECHNO-ECONOMIC OPTIMIZATION OF HYBRID CSP–PV SYSTEMS WITH ENERGY STORAGE FOR CONTINUOUS DME PRODUCTION IN CHILE

Nicholas Chandler[1,*], Johann Fetköter[2], Peter Schöttl[1], Silvan Feuerbach[1], Florian Nestler[1], Gregor Bern[1]

[1] *Fraunhofer Institute for Solar Energy Systems ISE, Heidenhofstraße 2, 79110 Freiburg im Breisgau, Germany*

[2] *Fraunhofer Institute for Energy Economics and Energy System Technology IEE, Joseph-Beuys-Straße 8, 34117 Kassel, Germany*

[*] *Corresponding author: nicholas.chandler@ise.fraunhofer.de*

Summary

Dimethyl ether (DME) is a promising low-carbon fuel, chemical intermediate, and platform molecule due to its clean combustion behavior, compatibility with LPG-like storage and transport infrastructure, and potential use in transport, heating, hydrogen storage, and chemical applications. This work assesses hybrid concentrating solar power (CSP) and photovoltaic (PV) systems with thermal and electrical storage for continuous CO_2-based methanol (MeOH) and DME production in northern Chile. The production chain extends a previously developed e-MeOH process model by adding DME synthesis, which increases the process heat demand and the need for stable downstream operation.

A high-resolution process-coupled simulation framework, combined with surrogate-assisted optimization, is used to compare four configurations: PV with battery energy storage (BESS) using either PEM or AEL electrolysis, and CSP–PV with BESS and an electric heater (EH) using either PEM or AEL electrolysis. The analysis is performed for Antofagasta and Mejillones with purchased electricity limited to 10% of total electrical demand. The results show that co-optimizing electricity and process heat supply is important for continuous DME production. In particular, CSP with thermal energy storage (TES) and an EH can provide dispatchable electricity, supply process heat, and convert otherwise curtailed PV electricity into useful thermal energy. Across the optimized cases, CSP–PV configurations reduce the levelized cost of DME (LCODME) by approximately 5.5% to 6.8% compared with the corresponding PV–only configurations, while improving downstream process utilization.

Keywords: Concentrating Solar Technologies (CST), Photovoltaics (PV), thermal energy storage, e-MeOH, e-DME, dynamic modeling, techno-economic optimization

Field of application for the findings: Sustainable Energy Infrastructure and Electrification.

Addressed audience: Solar-thermal and PV system designers, Power-to-X developers, and techno-economic analysts.

1. Introduction

Electricity-based DME, produced from renewable hydrogen and captured CO_2, is increasingly discussed as a low-carbon fuel and chemical intermediate. DME can be used as an LPG blendstock, a transport fuel for heavy-duty and marine applications, and a platform molecule for chemical production (Spazzafumo, 2021). Compared with several other synthetic fuels, DME benefits from relatively simple pressurized storage and transport requirements that are similar to existing LPG logistics (Florentinus and Hamelinck, 2012; Hsieh and Felby, 2017). Current large-scale DME production processes are generally operated under steady-state conditions. Therefore, a key challenge for renewable DME production, due to its intermittent nature, is ensuring a continuous supply of heat and electricity to hydrogen (H_2) production, MeOH production, and DME synthesis. This creates a strong motivation to investigate hybrid renewable energy systems that can provide both dispatchable electricity and process heat.

Hybrid systems that combine PV and CSP technologies are well suited for this task. PV can provide low-cost electricity during periods of high solar irradiance, while CSP with TES can shift solar energy to evening and night hours. In addition, CSP can provide process heat directly or indirectly through the thermal storage system. An EH can further improve the integration of the system by converting otherwise curtailed PV electricity into useful heat for the molten salt loop. This coupling between electricity and heat supply is especially relevant for fuel synthesis processes with continuous downstream operation.

Chandler et al. (2026a) developed an integrated techno-economic optimization framework for a 150 kt/a renewable methanol (e-MeOH) plant in Antofagasta, Chile. That study showed that hybrid CSP–PV systems with storage can reduce variability, improve process operability, and lower the levelized cost of methanol compared with configurations that rely only on PV and battery storage. The results also highlighted the importance of site-specific solar resources, component utilization, and the co-optimization of renewable generation, storage, and process capacities.

This work builds on that previous e-MeOH study by extending the production chain to continuous, conventional gas-phase DME production. The target production rate is 100 kt/a of DME, requiring upstream CO_2-based MeOH synthesis, MeOH distillation, and a dedicated DME synthesis step. Compared with the e-MeOH case, the DME plant has a higher constant process heat demand of approximately 22 MW_{th}, while the nominal electrical demand depends on the renewable energy and electrolysis configuration. Four configurations are evaluated: PV–BESS with proton exchange membrane (PEM) electrolysis, PV–BESS with alkaline electrolysis (AEL), CSP–PV–BESS–EH with PEM electrolysis, and CSP–PV–BESS–EH with AEL electrolysis.

The analysis is conducted for two sites in northern Chile, Antofagasta and Mejillones. For each site and configuration, high-resolution annual simulations are coupled with a surrogate-assisted optimization framework to identify cost-minimizing system designs with minimal reliance on the electrical grid. The optimization sizes the renewable generation system, storage units, selected process capacities, and dispatch-related parameters. The main objective is to minimize the levelized cost of DME (LCODME) while maintaining continuous production and limiting dependence on purchased electricity.

The main contribution of this work is the extension of a process-coupled CSP–PV optimization framework from e-MeOH to e-DME production. The system configuration considered in this study is shown in Figure 1. In particular, the paper evaluates how the additional DME synthesis step, increased process heat demand, and continuous downstream operation affect the optimal renewable energy system design. The results provide insight into the relative performance of PV–only and hybrid CSP–PV configurations, the influence of PEM and AEL electrolyzer technologies, and the potential role of thermal energy storage and electric heating in future solar-based Power-to-X plants.

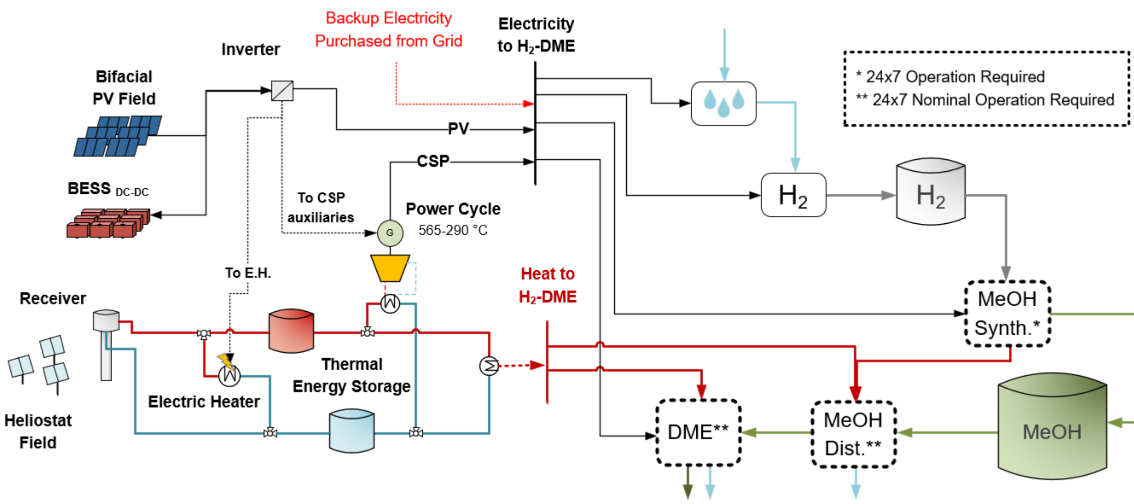

Fig. 1: Schematic of the H_2–MeOH–DME production chain and the CSP–PV configuration with EH and BESS integration for meeting electrical and thermal demands.

2. Methodology

This section describes the renewable energy system, H_2–MeOH–DME process model, heat and electricity supply, system coupling, techno-economic evaluation, and optimization framework.

2.1 Renewable Energy System Modeling

The simulations are performed using ColSim, Fraunhofer ISE's in-house transient thermal systems tool (Wittwer, 1999). ColSim has previously been applied to the modeling and validation of solar-thermal systems, the optimization of central receiver systems, and the simulation of hybrid CSP, PV, BESS, and electric heater configurations (Rohani et al., 2017; Schöttl et al., 2020; Chandler et al., 2026b). A key advantage of ColSim is its ability to generate high-resolution time series, enabling detailed analysis of the interactions between renewable energy generation, storage, process heat supply, and fuel production.

Two sites in northern Chile are considered: Antofagasta, located at 24.851°S, 69.908°W, and Mejillones, located at 22.771°S, 69.690°W. A typical meteorological year is generated from satellite data using Meteonorm v8 (Remund et al., 2020). Both locations have excellent solar resources. Antofagasta has an annual direct normal irradiance (DNI) of 3,186 kWh/m^2 and a global horizontal irradiance (GHI) of 2,653 kWh/m^2. Mejillones has an annual DNI of 3,320 kWh/m^2 and a GHI of 2,590 kWh/m^2.

2.1.1 Central Receiver Plant

For the CSP subsystem, a central receiver system (CRS) with a Rankine power block, dry cooling, and a two-tank direct molten-salt TES system is assumed. The TES can provide up to 20 full-load hours (FLH) of storage. The receiver operates between 290 and 565 °C. The optical components are modeled using the Raytrace3D suite (Schöttl et al., 2022, 2018; Branke and Heimsath, 2010). Heliostat field layouts are generated using the MUEEN radial-staggering algorithm (Leonardi et al., 2019).

The heliostat field and receiver are sized using the thermal multiple and optical multiple, which define the relative sizing of the receiver, power block, and heliostat field at the design point (Eceiza et al., 2023). These variables are optimized together with TES capacity and power block size.

In addition to electricity generation, heat from the CRS and TES is used to supply part of the H_2–MeOH–DME process heat demand. To ensure stable process heat availability, the minimum TES state of charge used for electricity generation is adjusted. This adjusted minimum state of charge limits discharge to the power block, thereby reserving part of the thermal storage capacity for process heat supply.

2.1.2 PV and BESS Technologies

The PV and BESS models follow the framework of Chandler et al. (2026a). High-performance bifacial PV modules on north-south single-axis trackers are assumed. The PV module parameters are based on the Trina Solar 705 NE module. The inverter converts PV-field DC power, P_{DC}, to AC power, P_{AC}, with an assumed conversion efficiency of 98.5%. PV oversizing is represented by the DC-to-AC ratio, which is defined as the ratio between installed PV DC capacity and inverter AC capacity.

A DC-coupled lithium-ion BESS is used for electrical storage. The BESS operates between 10% and 90% state of charge. A charge/discharge efficiency of $\eta_{c/d} = 92\%$ is assumed, resulting in an approximate round-trip efficiency of 85%. The BESS energy capacity, E_{BESS}, is treated as an optimization variable, while the maximum charge and discharge power is limited to 300 MW.

2.1.3 Electric Heater and Boiler Integration

A molten-salt EH is integrated into the renewable energy system and operates in parallel with the CRS. When excess PV electricity would otherwise be curtailed, the electricity can be directed to the EH and converted to thermal energy with an assumed efficiency of 99%. For CSP–PV configurations, the EH supplies heat to the molten-salt system and can support the process heat demand when thermal storage is depleted.

For PV–only configurations without thermal storage, an electric boiler with an assumed efficiency of 99% is used to provide the process heat demand (Ziarkash et al., 2025). In both configurations, purchased electricity may be used to operate the heater or boiler when renewable generation or TES are insufficient to meet the process heat demand.

2.2 H_2–MeOH–DME Modeling

The components of the H_2–MeOH–DME production chain are modeled as black-box units featured with parameterized performance curves obtained from AspenPlus-modeling and proprietary models as well as experimental data.. Their performance and cost parameters are taken from literature and adapted from the previous e-MeOH study, with additional assumptions for DME synthesis. The main process units are desalination, electrolysis, H_2 buffer storage, MeOH synthesis, MeOH buffer storage, MeOH distillation, and DME synthesis. In the production chain, H_2 produced by electrolysis is combined with captured CO_2 to produce crude MeOH. After purification by distillation, the MeOH is fed to a dedicated DME synthesis unit, which introduces an additional process-heat requirement.

Each black-box process can require electricity, heat, and feedstock. The conversion of inputs to products is represented by energy-to-product coefficients and feed conversion coefficients. Unless otherwise stated, component performance and costs are scaled linearly from baseline values. The main operating ranges and conversion coefficients are summarized in Table 1.

Tab. 1: Operating ranges and conversion coefficients by process. Values are adapted from Chandler et al. (2026a) and extended for DME. Part-load values for MeOH synthesis are given in Table 4 of Chandler et al. (2026a).

	Unit	**Desalination**[a]	**Electrolysis**[b]		**MeOH**[c]		**DME**[d]
			PEM	**AEL**	**Synth.**	**Dist.**	**Synth.**
Lifetime	a	30	7.9	9.9	30	30	30
Min. load	%	0	0	20	40	-	-
Max. load	%	100	100	100	100	100 (req.)	100 (req.)
$P_{El.}$ Req. (ξ_{el})	kWh_{el}/kg	0.0045	53.4	50.8	Variable	0.0	0.001
$P_{Th.}$ Req. (ξ_{th})	kWh_{th}/kg	0.0	0.0	0.0	0.0	0.681	0.765
Feed Req. (χ_{feed})	kg_{in}/kg_{out}	1.67	10.0	10.0	H_2: 0.12 CO_2: 0.88	1.57	MeOH: 1.40
Prod. heat (ϕ_{th})	kWh_{th}/kg	0.0	0.0	0.0	Variable	0.0	0.0

[a] Dirección de Estudios y Políticas Públicas (2015); Dambeck et al. (2020)
[b] Hemauer et al. (2023); Bram et al. (2024); Pichlmaier et al. (2021); Shin et al. (2023)
[c] Danish Energy Agency (2024); Feuerbach et al. (2026); Mbatha et al. (2026)
[d] Bîldea et al. (2017); Fortin et al. (2020)

2.2.1 Modeling of Individual Components

Reverse osmosis (RO) is assumed for seawater desalination. Since the required raw-water flow is modest compared with the overall plant scale, the raw water supply is included in the annual operating costs. Two electrolyzer technologies are considered: PEM and AEL. PEM electrolysis is assumed to offer full operational flexibility between 0% and 100% load, but it has higher capital costs and a shorter stack lifetime. AEL has lower capital costs and a longer stack lifetime, but its operation is constrained to a minimum load of 20%.

The MeOH synthesis unit uses CO_2 as the carbon source and operates between 40% and 100% of nominal load. Part-load performance is represented using load-dependent electricity demand and recoverable heat coefficients. The H_2 and MeOH buffer storage units are modeled using mass balances that are updated at each time step. Captured CO_2 is assumed to be purchased from a regional cement plant and transported to the production site. The assumed transport distance is 150 km for both sites.

The distillation unit receives a crude methanol stream and separates it into MeOH and water. The resulting distilled MeOH is then fed to the DME synthesis unit. Both the MeOH distillation and DME synthesis units are assumed to operate continuously at nominal load. Depending on the configuration and operating conditions, the required process heat is supplied by recovered synthesis heat, the CSP–TES system where applicable, the EH, or the electric boiler.

2.3 Modeling of the Combined System

The renewable energy system and the DME production chain are integrated into a single simulation framework, as illustrated in Figure 1. The main interfaces between the subsystems are electricity supply, process heat supply, and the operation of intermediate buffer storage. The combined system is operated to maintain continuous DME production while limiting purchased electricity.

2.3.1 Sizing of the H_2–MeOH–DME System

The principal operational constraint is continuous DME production at a nominal capacity of 100 kt/a. To satisfy this requirement, upstream units can be oversized relative to the DME design point. Oversizing allows the H_2 and MeOH buffers to be charged during periods of high renewable generation and discharged during periods of lower renewable availability.

A generic sizing multiple is introduced for each scalable process component. It is defined as the ratio between the installed capacity of component i and the design-point capacity required to meet the nominal DME production target:

$$\mathrm{SM}_i = \frac{C_i}{C_{i,\mathrm{DP}}} \tag{1}$$

Three main sizing multiples are applied. The MeOH synthesis sizing multiple, $\mathrm{SM}_{\mathrm{MeOH\,Synth.}}$, describes the oversizing of crude-MeOH production relative to the DME design point. The electrolyzer sizing multiple, $\mathrm{SM}_{\mathrm{Electro.}}$, scales the H_2 production capacity required to supply the oversized MeOH synthesis unit. The PV-inverter sizing multiple, $\mathrm{SM}_{\mathrm{Inv.}}$, scales the PV generation system relative to the nominal electrical demand of the H_2–MeOH–DME process.

For CSP–PV configurations, the CSP power block capacity is sized independently between 100 and 250 $\mathrm{MW_{el}}$. Excess inverter output can be stored in the BESS, converted to heat through the EH, used by the process units, or curtailed.

2.3.2 Operation of the Combined System

The combined plant is operated to maintain continuous DME production at nominal capacity. Upstream units and buffer storage are dispatched to ensure a steady feed to the downstream MeOH distillation and DME synthesis units while limiting purchased electricity. Figure 2 shows a representative multi-day time series.

When renewable electricity is abundant, MeOH synthesis operates at nominal load until the crude-MeOH buffer reaches its target state of charge. After this point, the electrolyzer prioritizes charging the H_2 buffer. If both buffers are sufficiently charged, process units reduce operation toward their minimum stable load where applicable, and excess renewable electricity is either stored, converted to heat, or curtailed.

In CSP–PV configurations, during periods of low solar resource, such as nighttime or cloudy conditions, the CSP subsystem can discharge TES through the power block to cover part of the electrical demand. The BESS is used to smooth short-term deficits and support transient operation. If renewable generation, BESS discharge, and TES-backed generation are insufficient, electricity is purchased from the grid, subject to the annual purchased electricity constraint.

The process heat demand is supplied by recovered heat from MeOH synthesis, heat from the CSP–TES system, the EH, or the electric boiler. In CSP–PV configurations, a portion of the TES capacity is reserved for process heat by adjusting the minimum TES state of charge used for electricity generation. If the TES is depleted, the EH may be operated using renewable or purchased electricity to maintain the process heat supply.

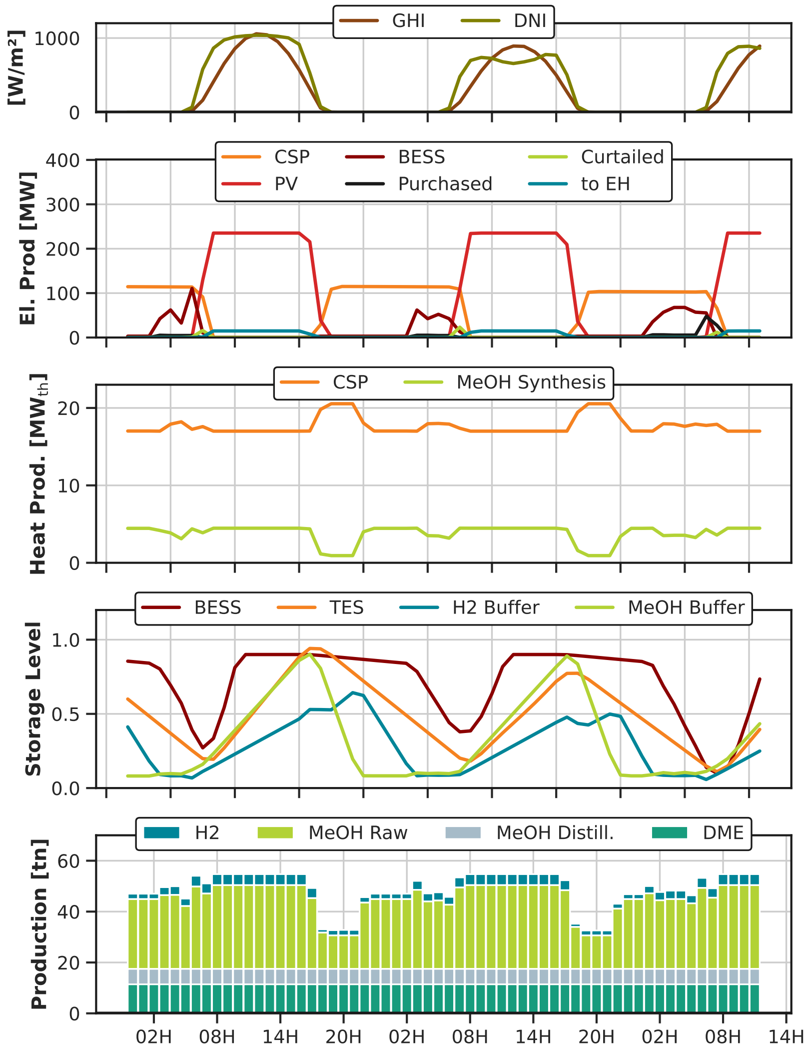

Fig. 2: Representative time series for a hybrid plant using a PEM electrolyzer. Top: GHI and DNI. Second and third: electrical and process heat flows by subsystem. Fourth: storage states of charge. Bottom: hourly product rates.

2.4 Techno-Economic Evaluation

The techno-economic evaluation includes the renewable energy system, storage technologies, electrolysis, process units, buffer storage, CO_2 supply, and purchased electricity. Specific cost assumptions for the renewable energy and H_2–MeOH systems are adapted from Chandler et al. (2026a). The additional installed cost for DME synthesis is calculated as $460\,003\,x^{0.283}$, where x is the installed DME synthesis capacity in kg/h. The corresponding annual operating cost is assumed to be 3% of the installed cost (Bîldea et al., 2017; Fortin et al., 2020).

A plant lifetime of 30 years and a real discount rate of 7% are assumed. Purchased grid electricity is priced at 155.44 €/MWh (BloombergNEF Climatescope, 2024). Components with shorter technical lifetimes, such as electrolyzer stacks, are replaced as required over the plant lifetime. Future replacement costs are discounted. Annual escalation of component costs, electricity prices, and CO_2 costs is not considered.

The main economic indicators are capital expenditure (CAPEX), annual operating expenditure (OPEX), levelized cost of electricity (LCOE), and LCODME. LCOE is calculated from the discounted system cost and the discounted renewable electricity generation over the plant lifetime. LCODME is calculated analogously using the annual DME production as the denominator. These equations are shown in Eq. 2 and Eq. 3.

$$\mathrm{LCOE} = \frac{\mathrm{CAPEX} + \sum_{t=1}^{N} \frac{\mathrm{OPEX}_t}{(1+r)^t}}{\sum_{t=1}^{N} \frac{E_0(1-d)^{t-1}}{(1+r)^t}} \quad (2)$$

$$\mathrm{LCODME} = \frac{\mathrm{CAPEX} + \sum_{t=1}^{N} \frac{\mathrm{OPEX}_t}{(1+r)^t}}{\sum_{t=1}^{N} \frac{M_{\mathrm{DME},t}}{(1+r)^t}} \quad (3)$$

In Eq. 2 and Eq. 3, the variable N is the economic lifetime of the plant, r is the real discount rate, and d is the annual PV degradation rate. For the LCOE calculation, E_0 denotes the renewable electricity generated in the first year of operation. For the LCODME calculation, $M_{\mathrm{DME},t}$ denotes the annual DME production in year t. Because continuous DME production is assumed, $M_{\mathrm{DME},t}$ remains constant over the plant lifetime.

The purchased electricity ratio, $C_{\mathrm{Pur.}}$, is used to quantify dependence on grid electricity. It is defined as the ratio between electricity purchased from the grid and the total electrical demand of the H_2–MeOH–DME process. In this study, the optimization is constrained to $C_{\mathrm{Pur.}} \leq 10\%$. Renewable electricity that cannot be used by the process, stored in the BESS, or converted to heat by the EH is treated as curtailed electricity. Purchased electricity used for process units, storage operation, and electric heat supply is included in this ratio.

2.5 Optimization Framework

The optimization minimizes LCODME subject to the purchased-electricity constraint $C_{\mathrm{Pur.}} \leq 10\%$, and only designs satisfying this constraint are retained. The integrated ColSim-based optimization framework shown in Figure 3 is extended to include the H_2–MeOH–DME production chain and DME-specific economic post-processing.

Candidate configurations are generated within the design limits listed in Table 2, sized, and simulated in ColSim over one year at a 300-second resolution. The resulting key performance indicators are used for economic evaluation and to train a random forest surrogate model. The surrogate model predicts the performance of additional candidate designs, which are ranked according to LCODME. The best-performing valid candidates are selected for crossover and mutation to generate new designs.

For the PV–only configurations, the optimization generated approximately 15 000 unique simulations. For the CSP–PV configurations, the optimization generated approximately 25 000 unique simulations because of the larger number of free design variables. The final reported configurations are the lowest-LCODME valid designs identified for each location, renewable energy configuration, and electrolyzer technology.

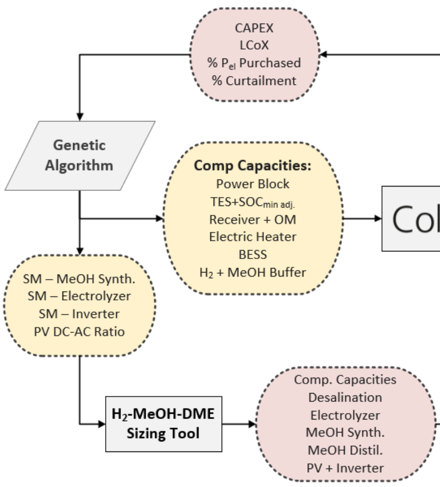

Fig. 3: Optimization toolchain: component sizing, ColSim simulation, economic post-processing, surrogate modeling, and evolutionary search, adapted from Chandler et al. (2026a).

Tab. 2: Optimization variable ranges and step sizes.

Component	Unit	Min	Max	Step
PV DC–AC ratio	–	0.9	3.0	0.05
$SM_{\mathrm{Inv.}}$	–	0.9	2.0	0.02
$SM_{\mathrm{Electro.}}$	–	1.0	2.0	0.02
$SM_{\mathrm{MeOH\ Synth.}}$	–	1.0	1.5	0.01
MeOH buffer	t	5	200	5
H_2 buffer	t	2	100	2
CSP PB	MW_{el}	100	250	25
CSP receiver	MW_{th}	100	800	10
CSP OM	–	0.9	1.5	0.05
CSP TES	FLH	2	20	0.5
$SOC_{\mathrm{min,\ adj}}$	%	5	30	0.5%
EH capacity	MW	10	200	5
BESS size	MWh	0	2000	50

3. Optimization Results and Discussion

Four technology configurations are evaluated and optimized for the two reference locations, Antofagasta and Mejillones. The configurations include PV with BESS and either PEM or AEL electrolysis, and CSP–PV with BESS, EH, and either PEM or AEL electrolysis. The objective is continuous DME production at minimum LCODME, subject to the purchased electricity constraint $C_{\mathrm{Pur.}} \leq 10\%$. Figure 4 shows the minimum-LCODME configurations for Antofagasta and Mejillones as a function of the renewable electricity share supplied to the H_2–MeOH–DME process. The figure also compares LCOE, CAPEX, first-year OPEX, and LCODME for the optimal designs at each renewable electricity share.

Across the candidate set, all four configurations are able to satisfy the purchased electricity constraint while maintaining continuous DME production. The minimum LCODME values range from 1.54 to 1.84 €/kg across all optimized cases. The lowest LCODME is obtained for the CSP–PV–AEL configuration in Antofagasta, with 1.54 €/kg. Across the optimal configurations, purchased electricity shares range from 2.8% to 4.9%, remaining below the imposed 10% limit in all cases. The optimized designs show that both PV–only and CSP–PV configurations can meet the continuous-production and purchased-electricity constraints at the selected sites.

For the optimal values shown in Figure 4, the LCODME for AEL-based configurations decreases from approximately 1.65 €/kg for PV–only systems to approximately 1.54 €/kg for CSP–PV systems. For PEM-based configurations, the corresponding decrease is from approximately 1.84 €/kg to approximately 1.73 €/kg. The optimized CSP–PV configurations therefore achieve approximately 5.5% to 6.8% lower LCODME than the corresponding PV–only configurations. This reduction cannot be attributed solely to lower LCOE. In several cases, PV–only configurations achieve lower electricity generation costs, but they require larger storage or process capacities to maintain continuous production.

The results show a consistent trade-off between CAPEX, OPEX, LCOE, and LCODME. As the renewable electricity share increases, total CAPEX generally increases because additional PV, CSP, BESS, TES, process capacity, or heat supply capacity is required. At the same time, first-year OPEX decreases because less electricity is purchased from the grid. The LCODME optimum therefore occurs at a balance between higher investment costs, lower operating costs, and improved process utilization.

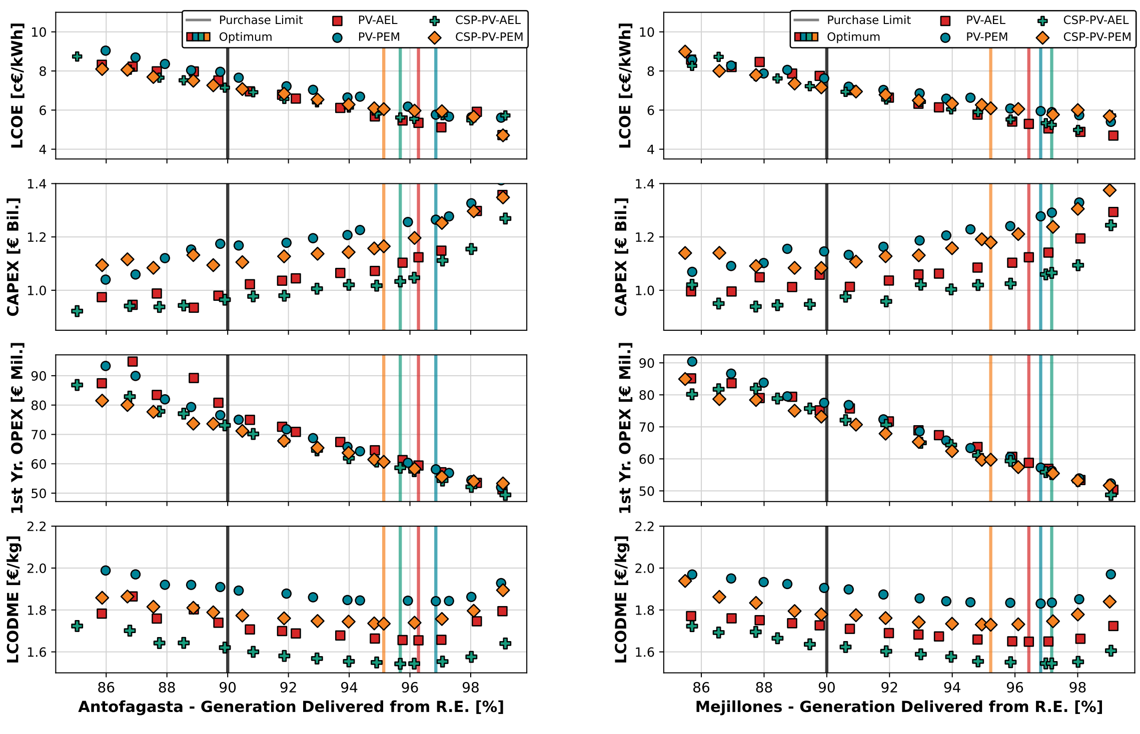

Fig. 4: LCOE, CAPEX, first-year OPEX, and LCODME for the minimum-LCODME configuration at each renewable-electricity share. Results are shown at 1% intervals of renewable electricity share ($100\% - C_{\mathrm{Pur.}}$), for (left) Antofagasta and (right) Mejillones. The gray bar indicates the 10% electricity purchase limit and the colored bars indicate the optimal configuration.

The difference between electrolyzer technologies also influences the optimal system design. AEL configurations generally achieve lower LCODME than PEM configurations under the assumed cost parameters because of their lower electrolyzer capital cost. Although PEM electrolysis offers greater flexibility during periods of fluctuating renewable generation, this advantage does not compensate for the higher electrolyzer cost in the optimized cases considered here.

Figure 5 shows the LCODME cost breakdown for the optimal configurations at both locations. The main cost drivers are the renewable energy system, electrolysis, CO_2 purchasing, and purchased electricity. The renewable energy system, including PV and BESS for PV-only configurations and CSP, PV, and BESS for CSP-PV configurations, accounts for approximately 36% to 38% and 38% to 40% of LCODME, respectively. Electrolysis contributes approximately 29% for PV-AEL, 33% to 35% for PV-PEM, 25% to 27% for CSP-PV-AEL, and 28% to 29% for CSP-PV-PEM. The higher renewable-system cost of the CSP-PV configurations is partly offset by lower electrolysis costs through improved electrolyzer utilization, together with process heat delivery and the dispatchability provided by TES-backed generation. The EH also allows excess PV electricity to be converted into thermal energy for direct process heat supply or storage in the molten-salt TES.

The improved dispatchability of the CSP–PV configurations also affects electrolyzer sizing and utilization, with optimized CSP–PV cases reaching approximately 68% to 84% electrolyzer utilization compared with 58% to 67% for PV–only cases. This indicates that TES-backed electricity generation and more stable renewable supply allow the electrolyzer to operate for a larger share of the year and closer to its nominal capacity. In contrast, PV–only configurations rely more strongly on daytime electricity production and require larger electrolyzer capacities to produce sufficient H_2 during periods of high PV output.

Purchased electricity contributes approximately 6% to 9% of LCODME across the optimal configurations. This cost contribution is distinct from $C_{\mathrm{Pur.}}$, which represents the share of total electrical demand supplied by purchased electricity and ranges from 2.8% to 4.9%. Some grid electricity is still favored in the cost-optimal solutions because eliminating nearly all electricity purchases would require additional renewable generation and storage capacity. The CSP-PV configurations do not consistently reduce purchased electricity compared with the corresponding PV-only systems. Instead, their economic advantage arises primarily from improved process utilization, dispatchable electricity generation, and integrated process heat supply.

CO_2 supply is another important cost driver. In this study, CO_2 is assumed to be sourced from a regional cement plant and transported 150 km to the DME production site. This highlights the importance of locating future e-fuel plants near suitable CO_2 sources, while also considering solar resource quality, port access, water availability, and grid connection requirements. Overall, both sites can support solar-based DME production under the imposed purchased-electricity constraint, with CSP–PV configurations providing the lowest LCODME by combining low-cost PV generation with dispatchable CSP electricity and thermal storage.

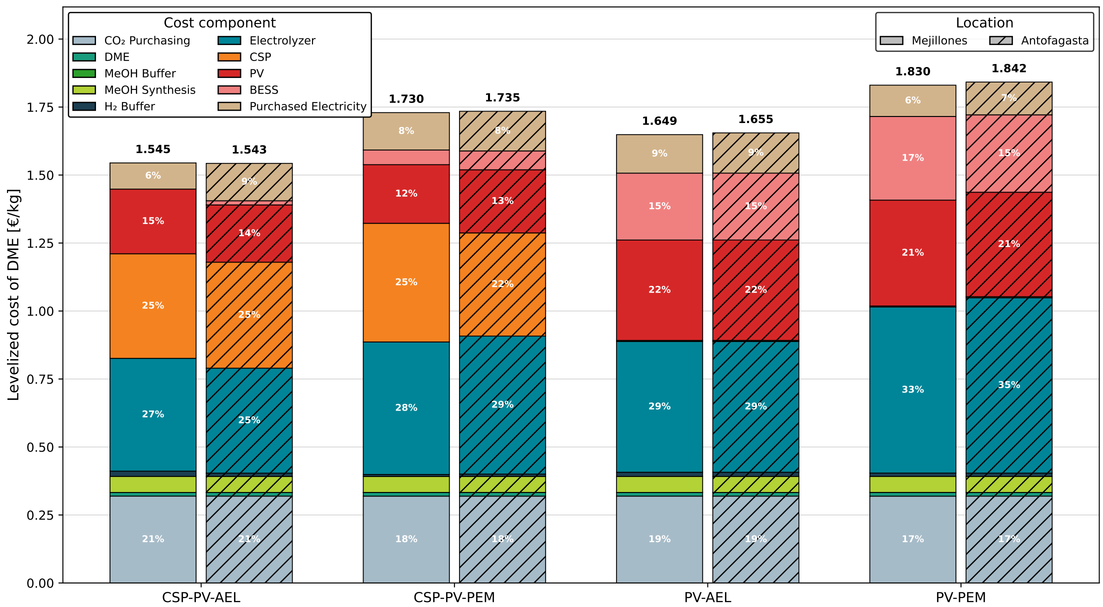

Fig. 5: Levelized cost of DME breakdowns for the four optimized configurations at both locations.

4. Conclusion

This work extends a previously developed e-MeOH optimization framework to continuous DME production in northern Chile. A coupled renewable energy and H_2–MeOH–DME process model was used to evaluate PV–only and hybrid CSP–PV configurations with either PEM or AEL electrolysis. The systems were optimized for two locations, Antofagasta and Mejillones, with the objective of minimizing LCODME while limiting purchased electricity to $C_{\text{Pur.}} \leq 10\%$.

The results show that hybrid CSP–PV systems can improve the operation and economics of continuous DME production. Compared with PV–only systems, the CSP–PV configurations benefit from dispatchable electricity generation, thermal energy storage, and direct or indirect process heat supply. The electric heater further improves system integration by converting otherwise curtailed PV electricity into useful heat. Together, these effects reduce the need for large battery capacities, improve downstream process utilization, and support continuous operation with purchased electricity remaining below 5% of total electrical demand in all optimized cases.

Across the optimized cases, CSP–PV configurations reduce LCODME by approximately 5.5% to 6.8% compared with the corresponding PV–only configurations. The AEL-based configurations also perform favorably under the assumed cost parameters because of their lower electrolyzer capital cost, despite their reduced operational flexibility compared with PEM electrolysis. The results further show that the lowest LCOE does not necessarily correspond to the lowest LCODME. Instead, the optimal system design depends on the combined effects of renewable generation cost, storage requirements, electrolyzer utilization, process heat supply, CO_2 cost, and purchased electricity.

Both Antofagasta and Mejillones are suitable locations for solar-based DME production, although future site selection should also consider actual CO_2 source locations, grid access, port access, water availability, local infrastructure, and potential industrial synergies. Future work should include a more detailed assessment of DME synthesis performance, electrolyzer operation under cold- and hot-start conditions, the use of local meteorological data, time-dependent electricity purchase prices, grid connection costs, certification of the renewable origin of purchased electricity, alternative CO_2 sourcing options, and alternative DME synthesis routes.

5. Declaration of Generative AI and AI-assisted technologies

During the preparation of this work, the authors used ChatGPT 5 to assist with grammar and spell checking and to rephrase sentences for readability. The authors reviewed and edited the content and take full responsibility for the published article.

6. Acknowledgements

The projects under which the work presented in this paper has been conducted were funded by the German Federal Ministry for Research, Technology and Space (BMFS, code 03SF0615A). The authors of this publication are responsible for its contents.

References

BloombergNEF Climatescope. Climatescope 2024: Chile. Online database, 2024. URL `https://www.global-climatescope.org/markets/chile`.

Mads Valentin Bram, Jesper Liniger, Sajjad Shoja Majidabad, Hamid Reza Shabani, Mavd P. R. Teles, and Xiaoti Cui. Challenges in Power-to-X: A perspective of the configuration and control process for e-methanol production. *International Journal of Hydrogen Energy*, 76:315–325, July 2024. doi: 10.1016/j.ijhydene.2024.05.273.

R. Branke and A. Heimsath. Raytrace3D-Power Tower: A novel optical model for central receiver systems. In *Proceedings of the 16th SolarPACES International Symposium*, Perpignan, France, September 2010.

C. S. Bîldea, R. Győrgy, C. C. Brunchi, and A. A. Kiss. Optimal design of intensified processes for DME synthesis. *Computers & Chemical Engineering*, 105:142–151, October 2017. ISSN 00981354. doi: 10.1016/j.compchemeng.2017.01.004.

Nicholas Chandler, Johann Fetköter, Peter Schöttl, Silvan Feuerbach, Florian Nestler, Christof Wittwer, and Gregor Bern. Techno-economic optimization of methanol production with hybrid solar technologies in chile. *Solar Energy*, 2026a. In press.

Nicholas Chandler, Daniel Marshal, Melisa Klein, Anna Heimsath, Christof Wittwer, Werner Platzer, and Gregor Bern. Optimizing high-resolution CSP-PV hybrid power plant configurations for Morocco: A techno-economic study. *Energies*, 19(10):2461, 2026b. doi: 10.3390/en19102461.

Hans Dambeck, Sven Kreidelmeyer, Almut Kirchner, and Marco Wünsch. Kosten und transformationspfade für strombasierte energieträger: Projekt "transformationspfade und regulatorischer rahmen für synthetische brennstoffe". Endbericht, Prognos AG, 2020.

Danish Energy Agency. Renewable fuels: Technology descriptions and projections for long-term energy system planning. Technical report, Danish Energy Agency, Copenhagen, 2024.

Dirección de Estudios y Políticas Públicas. Proyección del consumo de agua en la minería del cobre al 2026. Technical report, Comisión Chilena del Cobre, 2015.

Maitane Ferreres Eceiza, Peter Schöttl, Francisco Torres Sartori, Carlos Felbol, María Cerda, Thomas Fluri, and Gregor Bern. Techno-economic optimization of solar tower systems: Comparison of different sites in Chile. In *AIP Conference Proceedings*, volume 2815, page 030006, 2023. doi: 10.1063/5.0151233.

Silvan Feuerbach, , Florian Nestler, Achim Schaadt, Robert Szolak, Elias Frei, and Malte Gierse. Production of methanol and dimethyl ether via the ptx pathway: A techno-economic comparison of different process routes. *Submitted to Fuel*, 2026. Preprint.

Anouk Florentinus and Carlo Hamelinck. Potential of biofuels for shipping. Technical report, ECOFYS, 2012.

C. Fortin, N. Gianfolcaro, R. Gonzalez, J. Lohest, A. Lonneux, A. K. N. Siliki, T. Peiffer, R. Renson, and C. Schmitz. Dimethyl ether, A review of production processes and a modeling of the indirect route. Project report PROJ0012-1, University of Liège, 2020.

Johanna Hemauer, Sebastian Rehfeldt, Harald Klein, and Andreas Peschel. Performance and cost modelling taking into account the uncertainties and sensitivities of current and next-generation PEM water electrolysis technology. *International Journal of Hydrogen Energy*, 48(66):25619–25634, August 2023. doi: 10.1016/j.ijhydene.2023.03.050.

Chia-wen Carmen Hsieh and Claus Felby. Biofuels for the marine shipping sector. Technical report, IEA Bioenergy, 2017.

Erminia Leonardi, Lorenzo Pisani, Iñigo Les, Amaia Mutuberria Larrayoz, Shahab Rohani, and Peter Schöttl. Techno-economic heliostat field optimization: Comparative analysis of different layouts. *Solar Energy*, 180: 601–607, March 2019. doi: 10.1016/j.solener.2019.01.053.

Siphesihle Mbatha, Xiaoti Cui, Paulo Debiagi, Payam G. Panah, Raymond C. Everson, and Nicholas M. Musyoka. Detailed assessment of dynamic startup, shutdown, and flexibility of the adiabatic, gas-and water-cooled methanol fixed bed reactor: Comparison for power to methanol application. *Chemical Engineering Science*, 319:122280, 2026. doi: 10.1016/j.ces.2025.122280.

Simon Pichlmaier, Anika Regett, Stephan Kigle, Sofia Haas, Mario Feinauer, and Matthias Oswald. Ökobilanzen synthetischer kraftstoffe: Methodikleitfaden. Technical report, Forschungsstelle für Energiewirtschaft e. V., München, 2021. Methodikleitfaden zum Projekt Begleitforschung Energiewende im Verkehr (BEniVer).

J. Remund, S. Müller, M. Schmutz, and P. Graf. Meteonorm Version 8. In *Proceedings of the European PVSEC 2020*, September 2020.

S. Rohani, T. P. Fluri, F. Dinter, and Peter Nitz. Modelling and simulation of parabolic trough plants based on real operating data. *Solar Energy*, 158:845–860, December 2017. doi: 10.1016/j.solener.2017.10.023.

Peter Schöttl, Gregor Bern, De Wet Van Rooyen, Jonathan Flesch, Thomas Fluri, and Peter Nitz. Efficient modeling of variable solar flux distribution on Solar Tower receivers by interpolation of few discrete representations. *Solar Energy*, 160:43–55, January 2018. doi: 10.1016/j.solener.2017.11.028.

Peter Schöttl, Gregor Bern, De Wet Van Rooyen, José Antonio Fernández Pretel, Thomas Fluri, and Peter Nitz. Optimization of Solar Tower molten salt cavity receivers for maximum yield based on annual performance assessment. *Solar Energy*, 199:278–294, March 2020. doi: 10.1016/j.solener.2020.02.007.

Peter Schöttl, Gregor Bern, Peter Nitz, Francisco Torres, and Lina Graf. Raytrace3D by Fraunhofer ISE: Accurate and efficient ray tracing for concentrator optics. Technical report, Fraunhofer ISE, Freiburg, Germany, May 2022.

Haeseong Shin, Dohyung Jang, Sangdon Lee, Hyun-Seok Cho, Kyong-Hwan Kim, and Sanggyu Kang. Techno-economic evaluation of green hydrogen production with low-temperature water electrolysis technologies directly coupled with renewable power sources. *Energy Conversion and Management*, 286:117083, June 2023. doi: 10.1016/j.enconman.2023.117083.

G. Spazzafumo. *Power to Fuel: How to Speed Up a Hydrogen Economy*. Academic Press, London and San Diego, CA and Cambridge, MA and Oxford, 2021. ISBN 9780128232897.

Christof Wittwer. *ColSim: Simulation von Regelungssystemen in aktiven solarthermischen Anlagen*. Phd thesis, Karlsruhe Institut für Technologie, 1999.

Waris Ziarkash, Sven Bünning, Astrid Bensmann, Egbert Baake, and Richard Hanke-Rauschenbach. A comparative analysis of low-CO2 steam generation technologies. *Energy Conversion and Management: X*, 26: 101013, April 2025. doi: 10.1016/j.ecmx.2025.101013.